UNIVERSIDAD
NACIONAL
DE COLOMBIA

The switching control method for the nonlinear response of seismic surface based on the local T-S model

Yudong Jiang[1]*, Jinming Luo[2], Hojatallah Azarkhosh[3], Erjun Wu[3]

[1]College of college Engineering, Nanjing University of Aeronautics and Astronautics, Nanjing, 210016, China
[2]College of Automation, Shenyang Institute of Engineering, Shenyang, 110136, China
[3]College of civil and transportation engineering, Hohai University, Nanjing, China
*Corresponding author: luojinming0830@163.com; hojatazarkhosh@gmail.com

ABSTRACT

Based on the local T-S model, the switching control method for the nonlinear response of the seismic surface is studied, and the stiffness matrix of the composite interlayer element of viscoelastic damper and herringbone support is derived. The high-order single step ß method is applied to the nonlinear seismic response analysis and the instantaneous optimal active switching control. The local T-S model and controller are designed, and the approach and control of global nonlinear responses are realized through the multi-model switching control. The results show that the proposed method can accurately reflect the reduction of seismic ground load and the switching control of the main structure when the viscoelastic damper is installed. The switching control effect of the maximum spatial displacement becomes more and more obvious with the change of time history, and the control effect of all layers applying the switching control force is the most significant. Whether the controller is disturbed or not, it is always good and stable performance.

El método de control de conmutación para la respuesta no lineal de la superficie sísmica con base en el modelo local T-S

RESUMEN

Este artículo estudia el método de control de conmutación para la respuesta no lineal de la superficie sísmica con base en el modelo local T-S, y deriva la matriz de rigidez del elemento compuesto de capa intermedia del amortiguador viscoelástico y el soporte de espiga. El método ß de un solo paso de alto orden se aplica al análisis de respuesta sísmica no lineal y al control de conmutación activo óptimo instantáneo. El modelo local T-S y el controlador están diseñados, y el enfoque y el control de la respuesta global no lineal se realizan a través del control de conmutación multimodelo. Los resultados muestran que el método propuesto puede reflejar con precisión la reducción de la carga de tierra sísmica y el control de conmutación de la estructura principal cuando se instala el amortiguador viscoelástico. El efecto de control de cambio del desplazamiento espacial máximo se vuelve cada vez más obvio con el cambio del historial de tiempo, y el efecto de control de todas las capas que aplican la fuerza de control de cambio es el más significativo. Ya sea que el controlador esté alterado o no, siempre es un rendimiento bueno y estable.

Introduction

A large number of earthquake damage and existing records show that the earthquake will cause indelible damage to people's lives and property. With the development of China's national economy and the progress of science and technology, high-strength and light-weight building materials are widely used in building structures (Altukhov et al., 2018), the stiffness and damping of the structures are constantly reduced, and the building structures are more sensitive to seismic excitation. In order to reduce the seismic response of the building structure, in addition to studying the seismic design structure of the bearing system of the building structure itself (Zhang et al., 2017), some energy dissipation devices are set on the structure to increase the structural damping and consume the seismic energy through the nonlinear deformation of the energy dissipation materials, so as to reduce the seismic response of the main structure and effectively suppress the structural vibration (Zhang et al., 2016). Among these energy dissipation devices, the viscoelastic damper is the most concerned one (Ding et al., 2016), because it has the following advantages compared with other energy dissipation devices: as long as the structure starts to vibrate under minor interference, it can consume energy immediately (Zhang et al., 2018). Therefore, even in the case of small elastic vibration, it also plays the role of earthquake control. This makes it not only suppresses the seismic response of the structure but also avoid the problem of how the initial stiffness of the damper matches the lateral stiffness of the structure existing in other energy dissipation dampers (Wei et al., 2016); its "force-displacement" hysteretic curve is similar to the ellipse, so its energy dissipation is very strong (Bande & Choudhury, 2017).

Multi-model switching control is to approach the uncertainty and nonlinearity of response with multiple models. Based on multiple models, a controller (Viens et al., 2017) is established. Multiple controllers can be selected to act on the same control object, so as to effectively control complex response (Huang et al., 2018). It has nearly 40 years of development history. In recent ten years, some scholars have proposed multi-model control based on model switching. Many achievements have been made in theory and practice. The T-S fuzzy system is a kind of dynamic response fuzzy identification method proposed by Takagi and Sugeno. Its basic idea is to divide the input space into multiple fuzzy intervals, approximate each fuzzy interval with a linear model, and obtain the global model by local model interpolation. The larger the number of fuzzy rules is, the higher the precision is. However, when the number of rules of fuzzy reasoning is large, the calculation is complex and in some cases, no common positive definite matrix can be found to meet the stability conditions (Acerbi et al., 2016; Guo et al., 2017).

In this paper, multi-model switching control of nonlinear response based on the local T-S model is proposed. The model controller is designed, and the viscoelastic damper damping device is added to the building. Through the switching control, the switching control of the seismic surface response is realized.

Materials and methods

Combined stiffness matrix in the interlayer of viscoelastic damper and herringbone support

Stress-strain relationship of viscoelastic damping materials

Let and be the stress and strain of viscoelastic damping materials respectively. According to the research of Tsai and Lee, the stress-strain relationship satisfies the fractional derivative relationship

$$f(i\Delta t) = (G_0 + G_1)V(i\Delta t) + G_1 F(i\Delta t) \qquad (1)$$

Where $F(i\Delta t)$ is the original time effect of strain, and its expression is as follows:

$$F(i\Delta t) = \left[(i-1)^{1-T} + (1-i-T)i^{-T} \right] V(o) + \sum_{j=1}^{i=1} \left[(i-j-1)^{1-T} \right] V(j\Delta t) \qquad (2)$$

$$G_1 = \frac{A_0}{(\Delta t)^T \Gamma(2-T)} e^{-U\left[\int fdV + \theta(T-T_0) \right]} \qquad (3)$$

In the equation, G_0, A_0 and θ are all material parameters, which can be measured by experiments. According to equation (1), the stress-strain curve of viscoelastic damping material is an ellipse.

Stiffness matrix and switching control force vector of interlayer element

If the time interval is t, $t = i\Delta t$, according to the layer model, only one direction (x-direction) of vibration is analyzed at a time, it means the relative displacement of viscoelastic damper nodes along the X direction, then:

$$\{P_e\} = [B]^T \Delta P = (G_0 + G_1)\frac{A}{h}[B]^T[B]\{u\} + G_1 AF(i\Delta t)[B]^T \qquad (4)$$

In the equation, A is the acting area of the viscoelastic damper material; h is the thickness of the viscoelastic damper material; $\{P_e\}$ is the load vector of the viscoelastic damper node, and only $\{P_e\} = [P_{\times 1}, P_{\times 2}]^T$ along the X direction is considered; $\{u\} = \{u^1, u^2\}^T$ is the displacement vector of the viscoelastic damper element node.

From Equation 4, it can be seen that the load vector of the viscoelastic damper element is composed of two parts. The former one is similar to the load vector generated by ordinary elastic elements, and the latter one is the restoring force vector unique to viscoelastic damper elements, namely the vector of energy dissipation switching control force of the element.

Let $\{P_{ev}\}$ be the vector of energy dissipation switching control force of the element. According to equation (4):

$$\{P_{ev}\} = G_1 AF(i\Delta t)[B]^T = G_1 AF(i\Delta t)\begin{Bmatrix} -1 \\ 1 \end{Bmatrix} \qquad (5)$$

Let the element stiffness matrix of viscoelastic damper vibrate in one direction (X direction) be $[K_e]$, and it can get from equation (4):

$$[K_e] = (G_0 + G_1)A/h[B]^T[B] = A_0/h(G_0 + G_1)\begin{bmatrix} 1 & -1 \\ -1 & 1 \end{bmatrix} = K_1\begin{bmatrix} 1 & -1 \\ -1 & 1 \end{bmatrix} \qquad (6)$$

Where $K_1 = A_0/h(G_0 + G_1)$ is the element stiffness coefficient of the viscoelastic damper.

If the coefficient of element lateral stiffness matrix is K_2 and the lateral stiffness matrix of the element is $[Ks]$, then:

$$[Ks] = K_2\begin{bmatrix} 1 & -1 \\ -1 & 1 \end{bmatrix} \qquad (7)$$

Where, $K_2 = 2EA_s 1_2^2 / \left((1_2/2)^2 + h_2^2 \right)^{3/2}$; A_s, E, 1_2 and h_2 are the elastic modulus, cross-sectional area, span, and storey height of herringbone brace respectively. After the herringbone brace and viscoelastic damper are connected in series, the stiffness matrix of the interlayer element of the whole brace is as follows:

$$[K_{es}] = \frac{K_1 \cdot K_2}{K_1 + K_2}\begin{bmatrix} 1 & -1 \\ -1 & 1 \end{bmatrix} \qquad (8)$$

High-order single step ß method for nonlinear response analysis of seismic surface

Considering nonlinearity, the equation of motion of shear-type structure expressed by the relative displacement between layers under the action of the seismic surface load is as follows:

$$[M_1]\{\ddot{x}'\} + [C_1]\{\dot{x}'\} + \{f_e\} = -[M_1]\{A\} \cdot \ddot{x}_s \qquad (9)$$

Where, the restoring force of $[M_1]$, $[C_1]$ and $\{A\}$ is calculated according to the following equation:

$$\{f_e\} = [K_1]\{x'\}; f_{ej} = \overline{f}_{ej} - \overline{f}_{ej+1} = K_i^r x_i' + \overline{f}_{ef}^{\,B} - K_i^r x_B' \quad (10)$$

$$P_{pj}^r = \overline{f}_{ej}^{\,B} - K_i^r x_B' \quad (11)$$

Where, $\overline{f}_{ej}^{\,B}$ are the current restoring force and the previous switching control restoring force generated by the i-th layer; x_i' and x_B' are the current displacement and the previous switching control displacement of the i-th layer; P_{pj}^r and K_i^r are the plastic load and the current stiffness of the i-th layer respectively; according to equation (9), (10) and (11), the motion equation after entering the nonlinearity can be obtained as follows:

$$[M_1]\{\ddot{x}'\} + [C_1]\{\dot{x}'\} + [K_1^r]\{x'\} = -[M_1]\{A\}\ddot{x}_s - \{P_p^r\} \quad (12)$$

Where $[K_1^r]$ and $\{P_p^r\}$ represent the current stiffness matrix and plastic load matrix respectively.

According to Equation 12 and the assumption of the high-order single-step method, the equation for step-by-step integration can be obtained as follows:

$$
\begin{aligned}
\{x'\}_{n+1} &= [P_{11}]\{x'\}_n + [P_{12}]\{\dot{x}'\}_n + [Q_{12}][A]\{\ddot{x}\}_{gn} \\
&\quad + [R_{12}][A]\{\ddot{x}\}_{gn+1} - ([Q_{12}] + [R_{12}])[M_1^{-1}]\{P_p^r\} \\
\{\dot{x}'\}_{n+1} &= [P_{12}]\{x'\}_n + [P_{22}]\{\dot{x}'\}_n + [Q_{22}][A]\{\ddot{x}\}_{gn} \\
&\quad + [R_{22}][A]\{\ddot{x}\}_{gn+1} - ([Q_{22}] + [R_{22}])[M_1^{-1}]\{P_p^r\} \\
\{\ddot{x}'\}_{n+1} &= -[A]\{\ddot{x}\}_{gn+1} - [M_1^{-1}]([K_1^r]\{x'\}_{n+1} + [C_1]\{\dot{x}'\}_{n+1} + \{P_p^r\})
\end{aligned} \quad (13)
$$

A new instantaneous optimal algorithm for active switching control

The equation of motion for active switching control of structural seismic surface response is as follows:

$$[M]\{\ddot{x}(t)\} + [C]\{\dot{x}(t)\} + [K]\{x(t)\} = -[M]\{1\}\ddot{x}_g + [B]\{u\} \quad (14)$$

Where $\{u\}$ represents the $r \times 1$ order switching control force vector and $[B]$ represents the $n \times r$ order position matrix of switching control force action.

The index function has energy meaning, and any instantaneous index function can be taken as:

$$
\begin{aligned}
J &= \frac{1}{2}\{x\}^T W_1 [K]\{x\} + \frac{1}{2}\{\dot{x}\}^T (W_2 [M] + W_3 \Delta t [C])\{\dot{x}\} \\
&\quad + \frac{1}{2}([B]\{u\})^T [K]^{-1} [B]\{u\}
\end{aligned} \quad (15)
$$

Where, W_1, W_2 and W_3 are adjustable parameters of weight function.
Under the constraint of equation (14), let $\delta J_{n+1} = 0$, and then it can get:

$$[B]\{u\}_{n+1} = [D_1]\{x\}_n + [D_2]\{\dot{x}\}_n - [D_3]\{\ddot{x}\}_n + [D_4]\{1\}\ddot{x}_{gn+1} \quad (16)$$

In order to achieve closed-loop switching control, $[D_4]\{1\}\ddot{x}_{gn+1}$ is removed, so δJ_{n+1} of each step is no longer zero, that is, each step is only approximate optimization

$$[B]\{u\}_{n+1} = [D_1]\{x\}_n + [D_2][x]_n - [D_3]\{\dot{x}\}_n \quad (17)$$

From the above equation, the current applied switching control force $\{u\}_{n+1}$ can be obtained.

Controller design

The parallel distributed compensation algorithm (PDC) is used to design the local state feedback controller in the same region. The fuzzy control rule i in the same region is as follows:

$$if \quad z_1(t) \, is \, M_{i1} \, and \ldots and \, z_p(t) \, is \, M_{ip}, \, then \, u_i(t) = -K_i x(t) \quad (18)$$

Therefore, the region controller (e.g., the q-th region R_q, $q \in S$) is expressed as:

$$u_q = -\sum_{i=1}^{r} h_i(z(t)) K_i x(t) \quad (19)$$

The global controller $u(t)$ is actually the output of the current regional controller selected by the multi-model switching strategy, which can be expressed as $u(t) = u_{\sigma(t)}$, where $\sigma(t): [0,\infty) \to S = \{1,2,\ldots,s\}$ is a piecewise constant function depending on time t or state, $u_{\sigma(t)}$ is generated by switching in the controller set $\{u_1, u_2, \ldots, u_s\}$, and has the form $u_{\sigma(t)} = u_q, q \in S$, which can be further written as,

$$u_{\sigma(t)} = u_q = -\sum_{j=1}^{r} h_j(z(t)) K_j x(t) \quad (20)$$

According to equation (20), the closed-loop fuzzy control system can be deduced as follows:

$$\dot{x}(t) = \sum_{i=1}^{r} \sum_{j=1}^{r} h_i(z(t)) h_j(z(t)) [A_i - B_i K_j] x(t) \quad (21)$$

Stability of nonlinear response of multi-model switching control based on local T-S model

The Lyapunov stability results of the multi-model switching response are all based on the following assumptions: limited switching times between local models in a limited time (Wang, 2019).

For the convenience of the following proof, the switching function of the multi-model switching control is described by the characteristic function $v_q(z(t))$, namely:

$$v_q(z(t)) = \begin{cases} 1, & z(t) \in R_q \\ 0, & z(t) \notin R_q \end{cases}, q \in S = \{1,\ldots,s\} \quad (22)$$

It means that when the variable $z(t)$ is in the region q, the controller q corresponding to the current region u_q is selected by multi-model switching control. As a global controller $u(t)$, controllers in other regions do not work. Therefore, the global closed-loop control system and global controller of nonlinear reactive multi-model switching control based on local T-S model can be described as follows:

$$\dot{x} = \sum_{q=1}^{s} \sum_{i=1}^{r} v_q h_{qi} [A_{qi} x + B_{qi} u] \quad (23)$$

$$u = \sum_{q=1}^{s} \sum_{i=1}^{r} v_q h_{qi} K_{qj} x \quad (24)$$

Note: for the convenience of writing, x, v_q, h_{qi} and u are used to represent the corresponding $x(t)$, $v_q(z(t))$, $h_{qi}(z(t))$ and $u(t)$, the same below. Substituting equation (24) into equation (23), the global closed-loop fuzzy control system can be expressed as follows:

$$\dot{x} = \sum_{q=1}^{s} \sum_{i=1}^{r} \sum_{j=1}^{r} v_q h_{qi} h_{qj} [A_{qi} - B_{qi} K_{qj}] x \quad (25)$$

Lemma 1 If at any time t, the number of activated fuzzy rules is less than or equal to r, then there are:

$$\sum_{q=1}^{s}\sum_{i=1}^{r} v_q h_{qi}^2 - \frac{1}{r-1}\sum_{q=1}^{s}\sum_{i=1}^{r}\sum_{i=j} 2v_q h_{qi} h_{qj} \geq 0 \tag{26}$$

Prove According to this lemma:

$$\sum_{q=1}^{s}\sum_{i=1}^{r} v_q h_{qi}^2 - \frac{1}{r-1}\sum_{q=1}^{s}\sum_{i=1}^{r}\sum_{i=j} 2v_q h_{qi} h_{qj}$$

$$= \frac{1}{r-1}\sum_{q=1}^{s}\sum_{i=1}^{r}\sum_{i=1}^{r} v_q \left[h_{qi} - h_{qj}\right]^2 \geq 0 \tag{27}$$

From lemma 1, we can easily get lemma 2 as follows.

Lemma 2 If at any time t is less than or equal to η, $1 < \eta \leq 1$, then there are:

$$\sum_{q=1}^{s}\sum_{i=1}^{r} v_q h_{qi}^2 - \frac{1}{r-1}\sum_{q=1}^{s}\sum_{i=1}^{r}\sum_{i=j} 2v_q h_{qi} h_{qj} \geq 0 \tag{28}$$

Theorem It is assumed that at any time t, the number of activated fuzzy rules is less than or equal to η and . If there is a common symmetric positive definite matrix p and semi-positive definite matrix Q_q, the following linear matrix inequalities are obtained:

$$G_{qii}^T p + p G_{qii} + (\eta - 1) Q_q < 0 \tag{29}$$

$$\left(\frac{G_{qij} + G_{qji}}{2}\right)^T p + p\left(\frac{G_{qji} + G_{qji}}{2}\right) - Q_q \leq 0, i < j \tag{30}$$

Then the global closed-loop control system (25) based on the local T-S model is asymptotically stable. Where, $G_{qij} = A_{qj} - B_{qi} K_{qj}$.

Prove Let Lyapunov function $V(x) = x^T P x$, where P is a positive definite matrix. Along any trajectory of the closed-loop system (25), the derivative of $V(x)$ with respect to time is:

$$\dot{V}(x) = \sum_{q=1}^{s}\sum_{i=1}^{r}\sum_{j=1}^{r} v_q h_{qi} h_{qj} x^T \left[\begin{array}{c}\left(A_{qi} - B_{qi} K_{qj}\right)^T \\ p + p\left(A_{qi} - B_{qi} K_{qj}\right)\end{array}\right] x$$

$$= \sum_{q=1}^{s}\sum_{i=1}^{r} v_q h_{qi}^2 x^T \left[G_{qii}^T p + p G_{qii}\right] x \tag{31}$$
$$+ \sum_{q=1}^{s}\sum_{i=1}^{r}\sum_{i=j} 2v_q h_{qi} h_{qj} x^T G x$$

Where:

$$G = \left(\frac{G_{qij} + G_{qji}}{2}\right)^T p + p\left(\frac{G_{qji} + G_{qji}}{2}\right) \tag{32}$$

According to equation (29), (30) and Lemma 2, there are:

$$\dot{V}(x) \leq \sum_{q=1}^{s}\sum_{i=1}^{r} v_q h_{qi}^2 x^T \left[G_{qii}^T p + p G_{qii}\right] x + \sum_{q=1}^{s}\sum_{i=1}^{r}\sum_{i=j} 2v_q h_{qi} h_{qj} x^T Q_q x \leq$$

$$\sum_{q=1}^{s}\sum_{i=1}^{r} v_q h_{qi}^2 x^T \left[G_{qii}^T p + p G_{qii}\right] x + (\eta - 1)\sum_{q=1}^{s}\sum_{i=1}^{r} v_q h_{qi}^2 x^T Q_q x = \tag{33}$$

$$\sum_{q=1}^{s}\sum_{i=1}^{r} v_q h_{qi}^2 x^T \left[G_{qi}^T x^T p + p G_{qii} + (\eta - 1) Q_q\right] x$$

From equation (29), when $x(t) \neq 0$, there is $\dot{V}(x(t)) \neq 0$, so the global closed-loop control system (23) based on the local T-S model is asymptotically stable under the action of the global controller (24).

According to the stability conditions of the above theorem, based on LMI, the design of feedback controller and local feedback gain K_{qi} is to find a common symmetric positive definite matrix W, semi-positive definite matrix Y_q and matrix M_{qi}, which makes the following linear matrix inequalities to be enabled:

$$WA_{qi}^T + A_{qi}W - M_{qi}^T B_{qi}^T - B_{qi} M_{qi} + (\eta - 1) Y_q \quad 0 \tag{34}$$

$$WA_{qi}^T + A_{qi}W + WA_{qj}^T + A_{qj}W - M_{qj}^T B_{qi}^T - B_{qi} M_{qj} - M_{qi}^T B_{qj}^T$$
$$- B_{qj} M_{qi} - 2Y_q \quad 0, i j \tag{35}$$

Where $W = p^{-1}$, $M_{qi} = K_{qi}W$, $Y_q = WQ_q W$. With the help of the LMI toolbox in MATLAB, the feasp function is used to find the feasible solutions of W, Y_q and M_{qi} which satisfy the inequality. Then the local feedback gain K_{qi}, matrix P and Q_q are obtained, that is, $K_{qi} = M_{qi}W^{-1}$, $p = W^{-1}$, $Q_q = p Y_q p$.

Results

Project overview

A comprehensive building is a ten-story reinforced concrete frame structure, the height of the first to the third floor is 4.8m, the height of the fourth to the tenth floor is 4.2m, and the total height is 43.8m. The design of seismic crack resistance is 8 °, class II site. The viscoelastic damper is placed on the top of herringbone support, beam KL1 is 550mm × 250mm, KL2 is 300mm × 250mm, column section size is 500mm × 500mm, and steel support area is 4260 mm².

In the design of viscoelastic damper support, under the principle of reducing project cost, the stiffness of viscoelastic damper support should be increased as much as possible to ensure that viscoelastic dampers can produce enough restoring control force. In this design, ZN22 damping material produced by a factory is selected as the viscoelastic damping material, with material constants of G_0, A_0, and θ of 588, 2287, and 100.0, respectively. The unit is kN-m, and the area of single viscoelastic damping material is 0.7x0.7=0.49m², the thickness is 3mm, and the working temperature is 20 °C.

Calculation results and analysis

In order to verify the performance of the method in this paper, the time history analysis and calculation of the nonlinear seismic response of the structure supported by the viscoelastic damper (VED), the structure only supported by the same type of steel herringbone support and the original pure frame structure are carried out respectively. In the calculation, the El-Centro seismic surface acceleration record with a duration of 10.0s (its predominant period is 0.55s) is selected for the seismic surface wave. Considering the rare seismic surface action, the seismic surface acceleration X_g is 400gal. The calculation results of the maximum displacement of each floor of the three structures are shown in Figure 1.
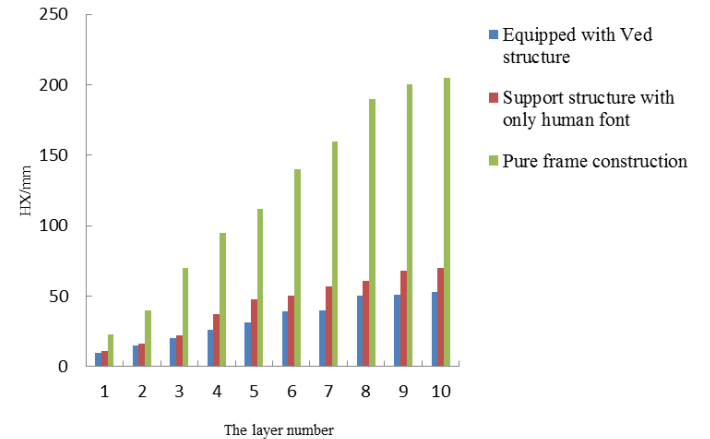
Figure 1. The horizontal displacement of each layer of the structure

Table 1 shows the cracking and entering plasticity of the three structural layers.

**Table 1.** Structural layer cracking and entering the plastic stage

Structural layer with Ved	Cracking	1 ~ 3 layers
	The inelastic	There is no
Only diagonally supported structural layers	Cracking	1 ~ 6 layers
	The inelastic	1 layer
Pure frame structure layer	Cracking	1 ~ 9 layers
	The inelastic	1 ~ 4 layers

It can be seen from Figure 1 and Table 1 that the displacement of the top layer and the shear force of the bottom layer of the structure with viscoelastic damper support is reduced by about 35% compared with that of the structure with herringbone support only, and about 70% compared with that of the pure frame structure; the number of cracking layers of the structure with viscoelastic damper herringbone support is reduced, the plastic stage of the structure layer is avoided, and the collapse of the structure is prevented. The viscoelastic damper can produce a strong energy dissipation control force, significantly increase the energy dissipation capacity of the whole structure, weaken the seismic ground load transmitted to the mainframe structure, and achieve the purpose of structural vibration switching control. The results show that this method can accurately reflect the seismic response of the structure with a viscoelastic damper, and it is a more practical and accurate calculation method.

Comparison of maximum interlayer displacement

The lateral stiffness K_1 of each floor of the ten-story complex building is 3.4×10^5, 3.26×10^5, 2.85×10^5, 2.71×10^5, 2.69×10^5, 2.43×10^5, 2.23×10^5, 2.07×10^5, 1.69×10^5, 1.37×10^5 kN/m. The layer damping coefficient C_i of each floor is 490, 467, 410, 386, 375, 348, 298, 274, 243, 196 kN·s/m respectively. The ground motion acceleration lasts for 8.5 s, and the maximum acceleration is 0.1g.

Fig. 2 shows the switching control effect of the proposed method on the seismic surface response by comparing the maximum displacement time history under the condition of free and no switching control with the displacement time history under the switching control imposed on the top layer of the proposed method (weight function is $W_1 = W_2 = W_3 = 168$).
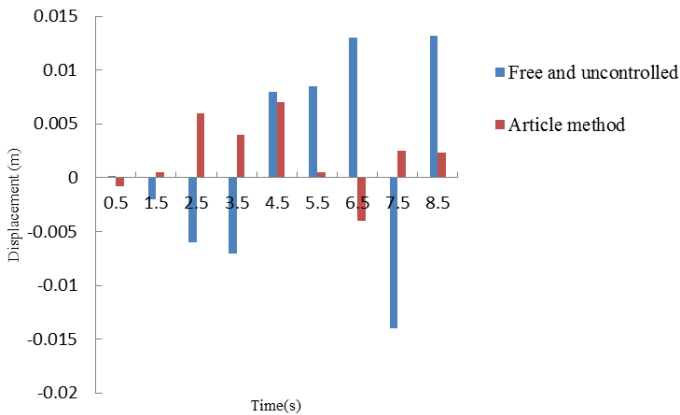
Figure 2. Maximum interlayer displacement response

It can be seen from Figure 2 that the switching control effect of the proposed method is more and more obvious with the change of time history. Here, the selection of weight function is selected through comparison. For different structures, the selection of weight function is different. Even for the same structure, different weight functions will lead to different switching control effects. When the weight function is not selected, it will lead to out of control.

Figure 3 shows the comparison of the maximum displacement time history of three different weight functions, where a is the applying switching control force on the top layer, and the weight function is $W_1 = W_2 = 168$, $W_3 = 0$; b is the applying switching control force on the top layer, and the weight function is $W_1 = W_2 = W_3 = 168$; c is the simultaneously applying switching control force on the fourth, sixth, eighth and 10-th layers, and the weight function is $W_1 = W_2 = 1000, W_3 = 10000$.
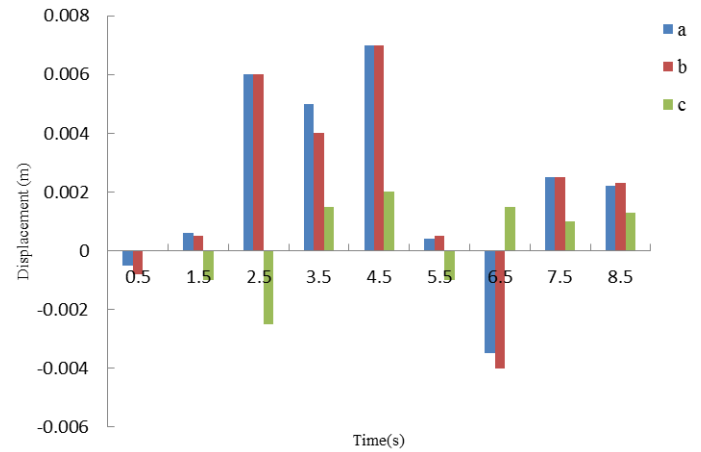
Figure 3. Maximum interlayer displacement response

It can be seen from Figure 3 that the change of W_3 in the weight function has no obvious effect on the control of the maximum displacement. The effect of multi-layer simultaneous application of switching control force is more obvious than that of only the top layer.

Figure 4 shows the calculation results of switching control force applied to some layers and all layers. Among them, c is the switching control force applied on the 4th, 6th, 8th, and 10th floor, with weight function of $W_1 = W_2 = 1000$ and $W_3 = 10000$; d is the switching control force applied on the 4th, 6th, 8th and 10th floor, with weight function of $W_1 = W_2 = 200$ and $W_3 = 2000$; e is the switching control force applied on the 10th floor, with weight function of $W_1 = W_2 = 200$ and $W_3 = 2000$.
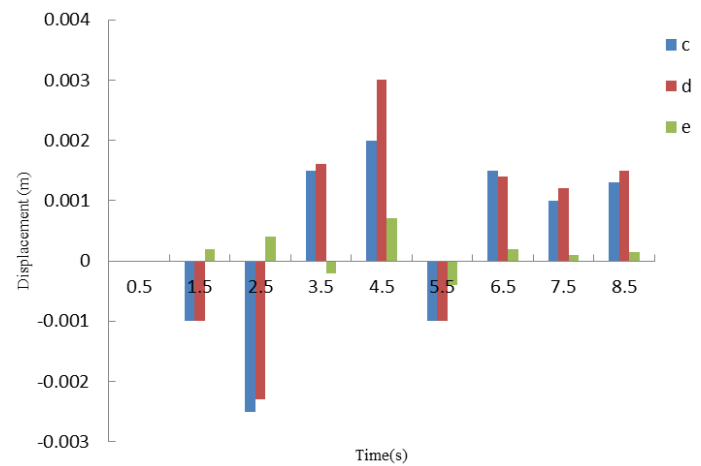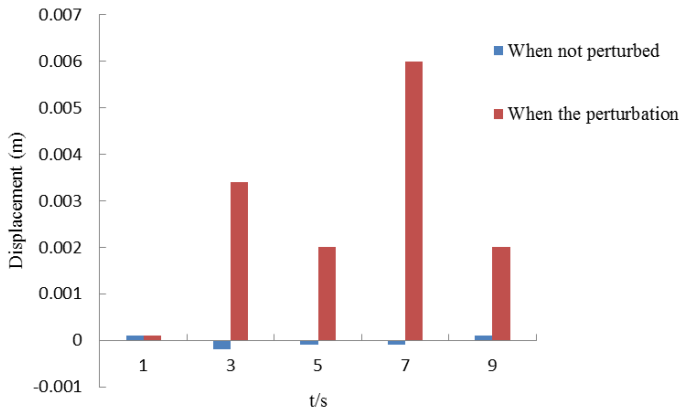

Figure 4. Maximum interlayer displacement response

It can be seen from Figure 4 that the selection of weight function has an impact on the control effect, and the control effect of switching control force applied to all layers is significant.

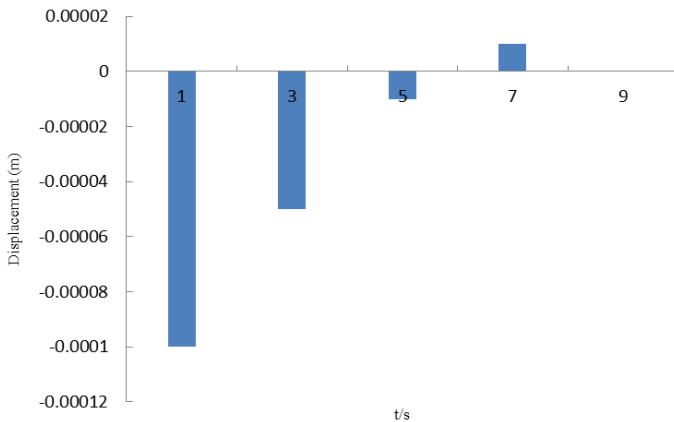**Maximum interlayer displacement response in a closed-loop state**

In the nominal case, that is, when there is no perturbation in the controller, the multi-model switching control method based on the local T-S model is applied to design the controller, and the reaction process is convergent

and stable; when there is a perturbation in the controller, the controller in the nominal case is still applied to realize the switching control for the reaction, and the reaction process is divergent and unstable. In both cases, the maximum interlayer displacement response in the closed-loop state is shown in Figure 5.

Figure 5. The closed-loop maximum inter-layer displacement response of conventional switching control

Assuming that the controller has the same additive perturbation as in the previous case, the controller is designed by the method in this paper. The maximum interlayer displacement response of the closed-loop state is shown in Figure 6, and the reaction process is convergent and stable.

Figure 6. In this paper, the closed-loop state maximum inter-layer displacement response of the controller is presented

It can be seen from Figure 5 and Figure 6 that when the controller itself does not have perturbation or is disturbed by perturbation, the controller adopting the method in this paper can obtain good performance and keep stable. The simulation results show the effectiveness of the proposed method.

Discussions

In the actual control process, the output variation range of the controller is limited (Yoon et al., 2016; Friederich et al., 2018), so its pole assignment is constrained when designing the controller. The multi-model switching control method proposed in this paper is used to divide the input space into several regions. Considering the actual constraints, poles can be flexibly allocated in different regions (Gao et al., 2016; Liu et al., 2016). Local controllers can be designed in each region, and then through the switching control, the approach and control of the overall nonlinear response can be realized, so that the controller can be avoided. The output saturation can also guarantee the convergence speed (Cheng et al., 2016). For the reaction with a wide range of parameters, the effectiveness will be more obvious. High-order single step β method can obtain better switching control effect than other instantaneous optimization algorithms (in the past, the switching control effect of other

algorithms is generally about 50% - 70%) (Li et al., 2016); adding damping term in the switching control index function has an impact on the switching control effect; for the value of weight function, there is the problem of optimal selection (Zhan et al., 2016); there is a problem of optimal switching control layer combination in multi-level switching control.

The proposed method can be applied to the design of controllers with a large range of response parameters and dynamic changes of subsystems. In addition to the application of this paper in the study of switching control of seismic surface response, it can also be applied to the air-to-air vehicle, for example. Because the air-to-air vehicle has the characteristics of time-varying, uncertainty and nonlinear coupling, the parameters of system response vary greatly, and a single dynamic model has no way to accurately describe the actual changes of the system (Yang & Long, 2016). Therefore, the method proposed in this paper can be used to approach the dynamic performance of the system, a multi-model controller is designed based on the multi-model, and multiple controllers can be selected to act on the same control object, so as to effectively control the complex system of an air space vehicle. The switching control of nonlinear response is still a problem that needs to be further studied. Because the nonlinear response model is difficult to establish and control, it can use multiple linear models to approach the nonlinear model, or use multiple simple nonlinear models to approach the complex nonlinear model, and then establish the multi model controller, which will have a good control effect on some nonlinear systems.

Conclusions

In this paper, a nonlinear response switching control method based on the local T-S model is proposed. By calculating the stress-strain relationship of viscoelastic damping materials, the stiffness matrix and switching control force vector of interlayer element, the herringbone support structure of viscoelastic damping material is applied to interlayer element, and the relative displacement of interlayer element is calculated by high-order single step β method combined with nonlinear seismic surface response analysis, which is used to represent the movement of shear structure under the seismic surface load. The controller is designed based on the local T-S model. By switching control, the nonlinear response of the whole seismic surface is controlled. In this paper, the switching control effect of the method for seismic surface response becomes more and more obvious with time. When the controller has additive perturbation, the convergence speed of the state response of the method in this paper is fast and stable, which shows the accuracy of the method in this paper for the switching control of seismic surface nonlinear response.

References

Acerbi, E., Fusco, N., Julin, V., & Morini, M. (2016). Nonlinear stability results for the modified Mullins-Sekerka and the surface diffusion flow. *Journal of differential geometry*, 113, 178-187.

Altukhov, V. I., Sankin, A. V., Sigov, A. S., Sysoev, D. K., Yanukyan, E. G., & Filippova, S. V. (2018). Schottky-Barrier Model Nonlinear in Surface-State Concentration and Calculation of the I–V, Characteristics of Diodes Based on SiC and Its Solid Solutions in the Composite Charge-Transport Model. *Semiconductors*, 52, 348-351.

Bande, G. R., & Choudhury, D. (2017). Seismic Passive Earth Resistance in Submerged Soils Using Modified Pseudo-Dynamic Method with Curved Rupture Surface. *Marine Georesources & Geotechnology*, 35, 930-938.

Cheng, X., Zhang, Q., Yu, X. J., Du, W., Liu, R., Bian, Q., Wang, Z., Zhang, T., & Guo, Z. (2016). Strike-slip fault network of the Huangshi structure, SW Qaidam Basin: Insights from surface fractures and seismic data.

Journal of Structural Geology, 94, 1-12.

Ding, X. J., Cheng, W., Li, Y., Wu, J. L., Li, X., Cheng, Q., & Ding, S. (2016). An enzyme-free surface plasmon resonance biosensing strategy for detection of DNA and small molecule based on nonlinear hybridization chain reaction. *Biosensors & Bioelectronics*, 87, 345-351.

Friederich, W., Hunzinger, S., & Wielandt, E. (2018). A note on the interpretation of seismic surface waves over three - dimensional structures. *Geophysical Journal International*, 143, 335-339.

Gao, R. M., Lv, T. H., & Hu, J. (2016). Explicit Expression of Limiting Spectral Density of High Dimensional Sample Covariance Matrices. *Journal of Jilin University (Science Edition),* 54, 499-505.

Guo, H. Y., Wang, L. F., Ye, W. H., Wu, J. F., & Zhang, W. Y. (2017). Weakly Nonlinear Rayleigh-Taylor Instability in Incompressible Fluids with Surface Tension. *Chinese Physics Letters*, 34, 60-63.

Huang, M., Kong, L. L., Cao, G. Q., Xiong, K., & Lishen, T. (2018). Analysis of short circuit failure of pouch-type lithium ion batteries. *Chinese Journal of Power Sources*, 42, 476-526.

Li, H. Y., Shi, P., & Yao, D. Y. (2016). Adaptive Sliding-Mode Control of Markov Jump Nonlinear Systems With Actuator Faults. *IEEE Transactions on Automatic Control*, 62, 1-1.

Liu, Y., Van der Neut, J., Arntsen, B., & Wapenaar, K. (2016). Combination of surface and borehole seismic data for robust target-oriented imaging. *Geophysical Journal International*, 205, 758-775.

Viens, L., Denolle, M., Miyake, H., Sakai, S., & Nakagawa, S. (2017). Retrieving impulse response function amplitudes from the ambient seismic field. *Geophysical Journal International*, 210, 210-222.

Wang, C. W. (2019). The application of VR laser technology in architectural layout. *Automation & Instrumentation*, 5, 234-237.

Wei, Y. F., Wang, X. W., Zheng, Z., Yang, M., & Xiao, J. (2016). Steady-state Modeling and Simulation for AC/DC Hybrid Power System Based on Modular Multilevel Converter . *Journal of Power Supply*, 14, 112-120.

Yang, X. L., & Long, Z. X. (2016). Seismic and static 3D stability of two-stage rock slope based on Hoek–Brown failure criterion. *Canadian Geotechnical Journal*, 53, 1-8.

Yoon, S. J., Kim, J. W., & Choi, W. Y. (2016). An Explicit Data Assimilation Scheme for a Nonlinear Wave Prediction Model Based on a Pseudo-Spectral Method. *IEEE Journal of Oceanic Engineering*, 41, 112-122.

Zhan, C. B., Luo, C., Ding, Z. K., & Jin, X. L. (2016). Research on Seismic Performance Prediction of High-rise Buildings. *Computer Simulation*, 33, 397-402.

Zhang, H. B., Guo, Q., Liang, L., Cao, C., & Shang, Z. (2017). A nonlinear method for multiparameter inversion of pre-stack seismic data based on anisotropic Markov random field. *Geophysical Prospecting*, 66, 461-477.

Zhang, J., Tang, Z. H., Ai, M. X., & Gui, W. (2018). Nonlinear modeling of the relationship between reagent dosage and flotation froth surface image by Hammerstein-Wiener model. *Minerals Engineering*, 120, 19-28.

Zhang, P., Qin, Z. C., & Lu, Z. (2016). An Analytical Model of Space Backbone Network Capacity for Space Information Transmission. *Journal of China Academy of Electronics and Information Technology*, 11, 66-72.